Highly Heterogeneous Depleted Mantle Recorded in the Lower Oceanic Crust

Sarah Lambart[1,2]*, Janne M. Koornneef[3], Marc-Alban Millet[1], Gareth R. Davies[3], Matthew Cook[1], C. Johan Lissenberg[1]

[1.] Cardiff university, School of Earth and Ocean Sciences, Cardiff, United Kingdom

[2.] University of Utah, Department of Geology and Geophysics, Salt Lake City, United States

[3.] Vrije Universiteit Amsterdam, Faculty of Science, Amsterdam, The Netherlands

The Earth's mantle is heterogeneous as a result of early planetary differentiation and subsequent crustal recycling during plate tectonics. Radiogenic isotope signatures of mid-ocean ridge basalts have been used for decades to map mantle composition, defining the depleted mantle end member. These lavas, however, homogenize via magma mixing and may not capture the full chemical variability of their mantle source. Here we show that the depleted mantle is significantly more heterogeneous than previously inferred from the compositions of lavas at the surface, extending to highly enriched compositions. We perform high spatial resolution isotopic analyses on clinopyroxene and plagioclase from lower crustal gabbros drilled on a depleted ridge segment of the northern Mid-Atlantic Ridge. These primitive cumulate minerals record nearly the full heterogeneity observed along the northern Mid-Atlantic Ridge, including hotspots. Our results demonstrate that substantial mantle heterogeneity is concealed in the lower oceanic crust and that melts derived from distinct mantle components can be delivered to the lower crust on a centimetre scale. These findings provide a starting point for re-evaluation of models of plate recycling, mantle convection, and melt transport in the mantle and the crust.

The mantle, Earth's largest geochemical reservoir and main source of volcanism, records the time-integrated history of recycling of oceanic lithosphere and its overlying sediments during the plate tectonic cycle[1,2]. The compositional heterogeneity thus generated within the mantle reflects this

recycling process[2,3]; determining the magnitude and length scale of this heterogeneity will enable a reconstruction of the recycling process and mantle convection, ultimately providing a window onto the dynamics of our planet. Mid-ocean ridge basalts (MORB) have been the primary tool to map geochemical heterogeneity of the oceanic upper mantle for decades[3-5]. However, because MORB mix in crustal magma chambers[6,7], the degree to which they are representative of its mantle source remains poorly constrained. Hence, the true heterogeneity of the MORB mantle source is uncertain, providing a significant barrier to understanding the magnitude and scale of recycled crust and the long-term evolution of the mantle.

One approach is to analyse the isotopic compositions of abyssal peridotites. These mantle samples may preserve a wider range of isotopic compositions than associated lavas[7-14]. However, they represent the melting residue of the MORB source, and potentially could have therefore lost the most fusible material[10] (pyroxenite, eclogite) thought to represent recycled, enriched, components[1]. Furthermore, interpretations are complicated by the common occurrence of recent refertilization in the lithospheric mantle beneath the ridge axis[11-13] and severity of alteration[7,11].

In this study, we overcome this problem by conducting crystal-scale Nd and Sr isotopic analyses on primitive cumulate minerals from the lower oceanic crust, and show that these cumulate minerals crystallised from heterogeneous melts extending to significantly more enriched compositions, than the associated MORB.

High magnitude small-scale heterogeneity in cumulate minerals

This study focuses on the Mid-Atlantic Ridge (MAR) segment north of the Atlantis Transform Fault (30°N), which is predominantly composed of volcanic rocks with isotopically depleted, normal mid-ocean ridge basalt (N-MORB) compositions[15]. Along the ridge-transform intersection, an uplifted dome of ultramafic and mafic plutonic rocks exposed by detachment faulting (the Atlantis Massif[16]) provides a window into the lower oceanic crust. Drill core of gabbroic cumulates (International Ocean Drilling Program, IODP Hole U1309D) yielded a detailed, 1415 m record of

53 the lower crust[16], which, along with the associated volcanic rocks, provides a unique opportunity to
54 compare the isotopic heterogeneity of melts delivered to the lower crust with those erupted onto the
55 seafloor. Results of Nd ($^{143}Nd/^{144}Nd$) and Sr ($^{87}Sr/^{86}Sr$) isotopic analyses on individual micro-
56 drilled clinopyroxene and plagioclase crystal domains from plutonic rocks of Hole U1309D are
57 shown in Fig. 1. We compare these data with whole rock isotopic compositions of diabase and
58 microgabbros collected on the same core, associated basalts flows (IODP Sites U1310 and U1311),
59 and Atlantic MORB and abyssal peridotite data from the literature, in Figs 1 and 2.

60 The results indicate that cumulate minerals: (1) are significantly more isotopically
61 heterogeneous than the associated diabase and lavas, exceeding the range of $^{143}Nd/^{144}Nd$ in MORB
62 from 30°N by a factor of seven (Fig. 1); (2) capture a significant proportion of mantle heterogeneity
63 reported in abyssal peridotites (Fig. 2a,b); and (3) record almost the full Nd isotopic heterogeneity
64 currently observed in all of North Atlantic MORB (including the enriched, plume-influenced
65 Azores platform, Iceland and Jan Mayen; Fig. 2a,b). Furthermore, Nd isotopic heterogeneity occurs
66 down to the centimetre scale, with plagioclase and clinopyroxene from individual samples
67 commonly not in isotopic equilibrium (Fig. 3). This small-scale heterogeneity can be explained by
68 multiple replenishments in the crystal mush leading to dissolution-crystallization episodes[17] and
69 juxtaposition of diverse populations of crystals[18]. At the grain scale, cores show more primitive
70 compositions (higher Mg# in clinopyroxene and anorthite content in plagioclase) than rims (see
71 Supplementary Fig. 1) suggesting that the cores crystallized from primitive melts upon melt
72 emplacement in the crust, while rims crystallized from late-stage percolating melts[19]. Once minerals
73 have formed, Nd diffusion is too slow to destroy grain-scale heterogeneity: at the solidus
74 temperature of a gabbro Nd zoning is preserved in calcic plagioclase on a 100μm-scale for more
75 than 10Myrs[20]; diffusion of Nd in clinopyroxene is even slower[21].

76 $^{87}Sr/^{86}Sr$ ratios are similarly variable. Most plagioclase data fall on the Sr-Nd isotopic data
77 array defined by global MORB (Supplementary Fig. 2) and could conceivably represent primary
78 values. However, clinopyroxenes typically record higher $^{87}Sr/^{86}Sr$ than plagioclase, suggesting

seawater alteration may have overprinted mantle signatures. Hence, we use only Nd isotope data for the interpretation.

A t-test shows no statistical difference between clinopyroxene and plagioclase $^{143}Nd/^{144}Nd$ but together, the cumulate minerals represent a distinct population compared to basalt, diabase and microgabbros (p-value <0.0002). However, the mean whole rock $^{143}Nd/^{144}Nd$ of the diabase, microgabbros, and associated basalt flows (0.513198±41) is within the 2σ error of that of the cumulate minerals (0.513138±187). Thus, there is no difference in the average compositions of the cumulate minerals relative to the basalt, diabase and microgabbros, but cumulate minerals record a larger variability. This indicates that cumulate minerals represent products of crystallization of small amount of melts that have undergone limited mixing before being delivered to the crust, whereas erupted MORB represent averages of much higher volumes of magmas that have been significantly mixed together at shallower depths.

Depleted mantle composition and temperature variations

These findings have important implications for both the magnitude and scale of heterogeneity of the upper mantle. The striking similarity of the Nd isotopic frequency distribution of cumulate minerals at Hole U1309D with that of North Atlantic MORB as a whole (Fig. 4) indicates that mantle heterogeneity beneath the Atlantis Massif is representative of the magnitude of heterogeneity in the North Atlantic basin. It follows that it is the proportion of recycled material in the aggregated magma, rather than the degree of isotopic enrichment of the recycled material in the source, that is responsible for variations in MORB isotopic compositions. If so, along-axis MORB variations should record the proportion of each component in MORB and in the mantle source along the axis. To assess this hypothesis, we use an adiabatic mantle melting model[22] to calculate: (i) the required proportion of recycled, material-derived melt to reproduce the Nd isotopic ratio of North Atlantic MORB (see Methods); (ii) the corresponding fraction of recycled material in the mantle source; and (iii) the thickness of oceanic crust generated along the ridge axis. It has been

105 suggested that MORB at the scale of a ridge segment (i.e., ~ 300 km) experienced common
106 differentiation processes[23]. Hence, we used the weighted average MORB compositions at a segment
107 scale. The melt derived from the recycled material has a higher Nd abundance than depleted
108 peridotitic melt[11]. Hence, adding a small amount of depleted peridotitic melt to the recycled
109 material-derived melt does not significantly affect the isotopic composition of the latter.
110 Conversely, even a small contribution of recycled material-derived melt can significantly modify
111 the isotopic composition of the depleted peridotite melt in such a way that the isotopic signature of
112 the depleted component is unlikely to be preserved in the cumulate minerals (see Methods). Hence,
113 we used the most enriched composition recorded in cumulates ($^{143}/^{144}$Nd = 0.512800±15) and the
114 most depleted composition recorded in North Atlantic abyssal peridotites ($^{143}/^{144}$Nd =
115 0.513662±18)[7] as isotopic compositions of the mantle end-members. Assuming the recycled
116 material is represented by recycled oceanic crust[24] (see Methods), the calculation yields a
117 proportion of recycled material-derived melt in locally averaged MORB of 27-59% (Fig. 2c). This
118 proportion is a function of both the proportion of recycled material in the source and the mantle
119 potential temperature (Supplementary Fig. 6a). To convert the proportion of recycled material-
120 derived melt in MORB to a proportion of recycled material in the mantle we performed three sets of
121 calculations: (1) we fixed the mantle potential temperature to T_P = 1300°C and calculated the
122 fraction of recycled material in the source required to explain the melt compositions; (2) we fixed
123 the fraction of recycled material in the mantle at 4% (i.e., the average fraction estimated in the first
124 set of calculations) and calculated the T_P required to explain the melt compositions; and (3) in a
125 hybrid model, we varied both the proportion of recycled material and the mantle potential
126 temperature. These calculations also yield melt volume, and hence crustal thickness. To evaluate
127 the validity of these models we compare the calculated crustal thickness for each ridge segment
128 with their average seafloor depth, a proxy for crustal thickness[25] (Fig. 2d and Supplementary Fig.
129 6b-e).

Varying the mantle potential temperature alone clearly failed to match the elevation profile by creating negative thickness anomalies around the major hot spots and producing crustal thickness variations much larger than those observed in the Atlantic basin[26]. Furthermore, it required a large range of mantle potential temperatures (1180-1440°C). It is worth noting, however, that varying the potential tempertature of a heterogeneous mantle can create a negative correlation between the contribution of the pyroxenite in the melt (Fig. 2c) and the crustal thickness (Supplementary Fig. 6b), as observed for the Vema lithospheric section[12]. Varying the proportion of recycled material alone did not reproduce small scale elevation variations on ridge segments far from the hot spots[27]. It also did not reproduce the bathymetry anomaly centered on Iceland. This anomaly is attributed to a significantly thickened crust (> 10 km)[26], likely produced by higher mantle potential temperature or high melt flux[28]. However, large-scale variations, such as the higher elevations of Jan Mayen and the Azores platform, are overall better correlated with thickness variations due to small variations of proportions of recycled material in the source rather than with thickness variations due to temperature variations. The best match is obtained by the hybrid model. Considering a variation of crustal thickness between 3 and 11 km[26], both compositional and elevation profiles are reproduced by varying T_P between 1245°C and 1367°C and the proportion of recycled material in the source between 3.2 and 8.5% (Fig. 2d; Supplementary Fig. 6d-e). Hence, our calculations support a model where higher proportion of recycled material in the source around the hot spot creates clear crustal thickness and chemical anomalies along most of the northern MAR without requiring large (>120°C) thermal variations.

Limited magma mixing during melt transport in the mantle

The finding of high-magnitude mantle heterogeneity delivered to the crust down to the centimetre scale requires that the MORB source is heterogeneous on a length scale smaller than the melting region. Variations of melt production have been observed along the northern MAR on a scale of 25-50 km[29]. If this length scale of variation is due to various proportions of mantle

156 components in the source region, then the scale of individual compositional domains must be
157 smaller. Short (10^{-3} to 10^{-2} m) Nd (and Sr) isotopic heterogeneity can persist over timescales of 10^9
158 yr in the solid mantle[30]. However, short mantle heterogeneities decrease the likelihood of extracting
159 the melt in (chemical) isolation, and melt-solid diffusion may destroy the isotopic signatures.
160 Hence, our study supports the prevalence of a kilometer size length scale of heterogeneity in the
161 MORB mantle source[12,31].

162 Crucially, the isotopic heterogeneity we observe in the Atlantis Massif cumulate minerals
163 provides strong evidence that heterogeneous melts are delivered to the lower crust without
164 significant mixing. Most melt generated by decompression melting is considered to be extracted
165 from the mantle through high-permeability channels[32,33]. It has previously been argued that
166 channelised melt transport is accompanied by significant mixing[31]. However, if this were the case, it
167 would quickly dilute heterogeneous isotopic compositions. Hence, our results suggest that magma
168 mixing inside the channels is limited. We propose that each mantle component could generate its
169 own network of channels to account for both preservation of isotopic heterogeneities and rapid
170 magma transport[34] (Fig. 5). Melt-rock reactions between recycled material-derived melt and
171 subsolidus peridotite favour a (near) closed-system evolution[35,36], and thermal diffusion can
172 nucleate channelization that preferentially samples melts from the most fusible component[37,38].
173 Eventually, magmas from the less fusible adjacent mantle can also start to focus together through
174 reactive or mechanical instabilities[30,33]. Such processes would discourage mixing between magmas
175 derived from each component and preserve extreme isotopic compositions (Fig. 5).

176 In conclusion, the isotopic heterogeneity revealed in the lower oceanic crust provides strong
177 evidence that the limited isotopic variability recorded in MORB is a consequence of crustal-level
178 mixing of melts form a highly heterogeneous source. Furthermore, our novel analytical approach
179 offers considerable potential to assess the full heterogeneity delivered to the crust across a range of
180 geodynamics settings. Finally, these new findings require re-evaluations of models for convective
181 thinning and stretching during mantle convection[39,40] and for melt migration through the mantle and

the crust[31,41] to account for greater isotopic heterogeneity and limited magma mixing in the depleted mantle.

References

1. Allègre, C.J., Turcotte, D.L. Implications of a two-component marble-cake mantle. *Nature* 323, 123-127 (1986).
2. Hofmann, A. W. Mantle geochemistry: the message from oceanic volcanism. *Nature* 385, 219–229 (1997).
3. Hart, S. R. Heterogeneous mantle domains: signatures, genesis and mixing chronologies. *Earth Planet. Sci. Lett.* 90, 273–296 (1988).
4. White, W. M. Sources of oceanic basalts: Radiogenic isotopic evidence. *Geology* 13(2), 115-118 (1985).
5. Cohen, R. S., Evensen, N. M., Hamilton, P. J., O'Nions, R. K. U–Pb, Sm–Nd and Rb–Sr systematics of mid-ocean ridge basalt glasses. *Nature* 283, 149-153 (1980).
6. Batiza, R. Inverse relationship between Sr isotope diversity and rate of oceanic volcanism has implications for mantle heterogeneity. *Nature* 309, 440-441 (1984).
7. Cipriani, A., Brueckner, H. K., Bonatti, E., Brunelli, D. Oceanic crust generated by elusive parents: Sr and Nd isotopes in basalt-peridotite pairs from the Mid-Atlantic Ridge. *Geology* 32, 657-660 (2004).
8. Stracke, A. et al. Abyssal peridotite Hf isotopes identify extreme mantle depletion. *Earth Planet. Sci. Lett.* 308, 359-368 (2011).
9. Warren, J. M. Global variations in abyssal peridotite compositions. *Lithos* 248, 193-219 (2016).
10. Salters, V.J.M., Dick, H.J.B. Mineralogy of the mid-ocean-ridge basalt source from neodymium isotopic composition of abyssal peridotites. *Nature* 418, 68-72 (2002).

11. Warren, J. M., Shimizum N., Sakaguchi, C., Dick, H. J. B., Nakamura, E. An assessment of upper mantle heterogeneity based on abyssal peridotite isotopic compositions. *J. Geophys. Res. Solid Earth* 114, B12203 (2009).
12. Brunelli, D., Cipriani, A., Bonatti, E. Thermal effects of pyroxenites on mantle melting below mid-ocean ridges. *Nature Geosci.* 11, 520-525 (2018).
13. Mallick, S., Dick, H. J., Sachi-Kocher, A., Salters, V. J. Isotope and trace element insights into heterogeneity of subridge mantle. *Geochem. Geophys. Geosyst.* 15(6), 2438-2453 (2014).
14. Snow, J. E., Hart, S.R., Dick H.J.B. Nd and Sr isotope evidence linking mid-ocean-ridge basalts and abyssal peridotites. *Nature* 371, 57-60 (1994).
15. Gale, A., Dalton, C. A., Langmuir, C. H., Su, Y., Schilling, J. G. The mean composition of ocean ridge basalts. *Geochem. Geophys. Geosyst.* 14(3), 489–518 (2013).
16. Blackman, D. K. et al. Drilling constraints on lithospheric accretion and evolution at Atlantis Massif, Mid□Atlantic Ridge 30°N. *J. Geophys. Res.* 116, B07103 (2011).
17. Leuthold, J., Lissenberg, C. J., O'Driscoll, B., Karakas, O., Falloon, T., Klimentyeva, D. N., Ulmer, P. Partial melting of lower oceanic crust gabbro: constraints from poikilitic clinopyroxene primocrysts. *Frontiers in Earth Sci.* 6, 15 (2018).
18. Schleicher, J. M., Bergantz, G. W. The mechanics and temporal evolution of an open-system magmatic intrusion into a crystal-rich magma. *J. Petrol.* 58(6), 1059-1072 (2017).
19. Lissenberg, C. J., MacLeod, C. J. A reactive porous flow control on mid-ocean ridge magmatic evolution. *J. Petrol.* 57(11-12), 2195-2220 (2016).
20. Cherniak, D. J. REE diffusion in feldspar. *Chem. Geol.* 193(1-2), 25-41 (2003).
21. Van Orman, J. A., Grove, T. L., Shimizu, N. Rare earth element diffusion in diopside: influence of temperature, pressure, and ionic radius, and an elastic model for diffusion in silicates. *Contrib. Mineral. Petrol.,* 141(6), 687-703 (2001).
22. Lambart, S. No direct contribution of recycled crust in Icelandic basalts. *Geochem. Perspect. Lett.* 4, 7-12 (2017).

232 23. Shorttle, O. Geochemical variability in MORB controlled by concurrent mixing and crystallization.
233 *Earth Planet. Sci. Lett.* 424, 1-14 (2015).
234 24. Hart, S., Blusztajn, J., Dick, H. J. B., Meyer, P. S., Muehlenbachs, K. The fingerprint of
235 seawater circulation in a 500-meter section of ocean crust gabbros. *Geochim. Cosmochim. Acta*
236 63, 4059–4080 (1999).
237 25. Barth, G. A., Mutter, J. C. Variability in oceanic crustal thickness and structure: Multichannel
238 seismic reflection results from the northern East Pacific Rise. *J. Geophys. Res.*101(B8), 17,951-
239 17,975 (1996).
240 26. Wang, T., Lin, J., Tucholke, B., Chen, Y. J. Crustal thickness anomalies in the North Atlantic
241 Ocean basin from gravity analysis, *Geochem. Geophys. Geosyst.* 12, Q0AE02 (2011).
242 27. Langmuir, C. H., Klein, E. M., Plank T. Petrological systematics of mid-ocean ridge basalts:
243 constraints on melt generation beneath ocean ridges. *Geophys. Monogr. Ser.* 71, 183-280
244 (1992).
245 28. Maclennan, J. Concurrent mixing and cooling of melts under Iceland. *J. Petrol.* 49, 1931–1953
246 (2008).
247 29. Wang, T., Tucholke, B. E., Lin., J. Spatial and temporal variations in crustal production at the
248 Mid-Atlantic Ridge, 25°N–27°30′N and 0–27 Ma, *J. Geophys. Res. Solid Earth,* 120, 2119–
249 2142 (2015).
250 30. Kogiso, T., Hirschmann, M. M., Reiners, P. W. Length scales of mantle heterogeneities and their
251 relationship to ocean island basalt geochemistry. *Geochim. Cosmochim. Acta* 68, 345-360 (2004).
252 31. Liu, B., Liang, Y. The prevalence of kilometer-scale heterogeneity in the source region of
253 MORB upper mantle. *Sci. Adv*. 3, e1701872 (2017).
254 32. Kelemen, P. B., Shimizu, N., Salters, V. J. M. Extraction of mid-ocean-ridge basalt from the
255 upwelling mantle by focused flow of melt in dunite channels. *Nature* 375, 747-753 (1995).

33. Spiegelman, M., Kelemen, P. B., Aharonov, E. Causes and consequences of flow organization during melt transport: The reaction infiltration instability in compactible media. *J. Geophys. Res.* 106(B2), 2061-2077 (2001).

34. Elliott, T., Spiegelman, M. 4.15 – Melt migration in oceanic crustal production: A U-Series Perspective. In Holland, H. D. & Turekian, K. K. (eds) *Treatise on Geochemistry*, 2nd edn. Oxford: Elsevier, pp. 543-581 (2014).

35. Lambart, S., Laporte, D., Provost, A., Schiano, P. Fate of pyroxenite-derived melts in the peridotitic mantle: thermodynamical and experimental constraints. *J. Petrol.* 53 (3), 451–476 (2012).

36. Yaxley, G., Green, D.H. Reactions between eclogite and peridotite: mantle refertilisation by subduction of oceanic crust. *Schweizerische Mineralogische und Petrographische Mitteilungen* 78(2), 243-255 (1998).

37. Weatherley, S. M., Katz, R. F. Melting and channelized magmatic flow in chemically heterogeneous, upwelling mantle, *Geochem. Geophys. Geosyst.* 13, Q0AC18 (2012).

38. Weatherley, S. M., Katz, R. F. Melt transport rates in heterogeneous mantle beneath mid-ocean ridges. *Geochim Cosmochim Acta*, 172, 39-54 (2016).

39. Anderson, D. L. The scales of mantle convection. *Techtonophysics* 284, 1-17 (1998).

40. Stixrude, L., Lithgow-Bertelloni, C. Geophysics of Chemical Heterogeneity in the Mantle. *Annu. Rev. Earth Planet. Sci.* 40, 569-595 (2012).

41. Wanless, V. D., Shaw, A. M. Lower crustal crystallization and melt evolution at mid-ocean ridges. *Nature Geosci.* 5, 651-655 (2012).

42. Delacour, A., Früh-Green, G. L., Frank, M., Gutjahr, M., Kelley, D. S. Sr- and Nd-isotope geochemistry of the Atlantis Massif (30°N, MAR): Implications for fluid fluxes and lithospheric heterogeneity. *Chem. Geol.* 254, 19-35 (2008).

43. Lehnert, K., Su, Y., Langmuir, C., Sarbas, B., Nohl, U. A global geochemical database structure for rocks. *Geochem. Geophys. Geosyst.* 1, 1012 (2000).

Materials & Correspondence. Correspondence and requests for materials should be addressed to Sarah Lambart (sarah.lambart@utah.edu).

Acknowledgments: This work was supported by the European Union's Horizon 2020 research and innovation programme (Marie Skłodowska-Curie grant agreement No. 663830) and National Science Foundation (EAR-1834367) to S.L. We thank Duncan Muir, Iain McDonald, Tony Oldroyd and Max Jansen for their assistance on the SEM, LA-ICP-MS, with sample preparation and in using the micromill, respectively. We also thank V. Salters and an anonymous reviewer for their constructive reviews that greatly improved the manuscript.

Author contributions: JL designed the study. SL and JL wrote the manuscript with input from MAM, JK and GD. SL and JL selected the samples. SL and MC performed the element maps. SL performed trace element analyses and geochemical modelling. SL and JL performed micro-milling, and SL, JL, MAM and JK performed column chemistry and isotopic analyses.

Competing interests. The authors declare no competing interests.

Figure captions:

Fig. 1. Isotopic compositions of Atlantis Massif cumulate minerals. $^{87}Sr/^{86}Sr$ (a) and $^{143}Nd/^{144}Nd$ (b) ratios of clinopyroxene (green) and plagioclase (blue) cores of cumulate gabbroic rocks from IODP Hole U1309D, compared with whole rock (WR) isotopic analyses performed in this study (red symbols) and on gabbroic rocks recording less than 40% alteration[42] (black crosses). The grey bands represent the compositional variability of MORB analysed in this study and reported in the literature (PetDB database[43]) at the same latitude (30°N±1°). Error bars: 2SEE; mbsf = metres below seafloor.

Fig. 2. Isotopic compositions of cumulate minerals, abyssal peridotites and MORB along the northern MAR and results of geochemical modeling. a-b. $^{87}Sr/^{86}Sr$ (a) and $^{143}Nd/^{144}Nd$ (b) ratios measured in this study, in MORB (PetDB Database[43]) and in abyssal peridotites[7,12,13] from the northern MAR. Red dotted lines show the latitude of the major hotspots affecting MORB compositions[15]. Error bars: 2 SEE. In (b), the vertical dashed lines show the isotopic compositions of the two mantle components used in calculations and the yellow circles are the average MORB compositions per ridge segment. **c.** Calculated fraction of recycled, material-derived melt in the averaged MORB. **d.** Comparison of the calculated crustal thicknesses generated by varying the proportion of recycled material and the potential temperature (dashed green line) with the averaged elevations of the collected MORB (orange line).

Fig. 3. Intrasample heterogeneity. $^{143}Nd/^{144}Nd$ ratios of plagioclase (black circles) and clinopyroxene (colored circles) as a function of the anorthite (An) content of the plagioclase in the sample. Analyses from individual samples are connected by black tie lines. The blue line and field show the average and 2σ composition of the cumulate minerals. The red line and field show the average composition and 2σ of MORB (basalts, diabase and microgabbros).

Fig. 4. Frequency distribution of Nd isotopic compositions. Comparison between plagioclase and clinopyroxenes from primitive cumulates (this study) and North Atlantic MORB (grey: all data; yellow: MORB not affected by hot spots[15]).

Fig. 5. Illustration of magma delivery from a two-component mantle to the crust. The fusible and enriched recycled material (in red) starts to melt at higher pressure than the depleted peridotite. Both lithologies nucleate their own network of high-permeability channels, facilitated by melt-rock reaction[35,36] and thermal diffusion[37,38], and by mechanical[30] and/or chemical[33] instabilities, respectively. Generation of separate networks limits magma mixing and help to deliver a larger isotopic variability to the crust. The shallowest axial magma chamber host a larger volume of

magma where mixing and crystallization continue, resulting in the loss of much of the primary mantle diversity.

Methods

Geological setting and sample selection

The Atlantis Massif is a 1.5-2 Myr old oceanic core complex on the western rift flank of Mid-Atlantic Ridge 30°N. IODP Sites U1309, U1310 and U1311 were drilled during Expeditions 304 and 305. The main hole, Hole U1309D, penetrated 1415.5 mbsf and recovery averaged 75%. Over 96% of Hole U1309D is made up of gabbroic rock types, which are amongst the most primitive as well as freshest plutonic rocks known from the ocean floor[16].

We selected 74 samples from the core U1309D samples to cover the entire drill hole, including 28 olivine gabbros, 8 troctolites, 7 olivine-rich troctolites, 11 gabbros, 4 oxide gabbros, 2 gabbronorites, 6 microgabbros and 7 diabases. We also collected 9 basalt and glass samples recovered at IODP sites U1310 and U1311.

Element maps and selection of mineral for isotopic analyses

Forty of the selected samples were polished and carbon-coated to perform major and minor element maps. Element maps were obtained at Cardiff University on a Zeiss Sigma HD FEG-SEM equipped with dual Oxford Instruments X-max 150 mm^2 energy dispersive silicon drift detectors. We used an acceleration voltage of 20 kV and a dwell time of 9 ms. The beam current and aperture were adjusted to obtain optimum output count rates of ~410,000 cps, enabling rapid mapping of large proportions of the samples at high spatial resolution (step size 20 μm). Raw counts were background corrected using Oxford Instrument's AZtec software, which was then used to generate multi-element maps.

From these element maps, we selected primitive, fracture and inclusion free, plagioclase (high anorthite, An, content) and clinopyroxene (high Mg# and low TiO_2/Cr_2O_3 ratio) cores for

358 micromilling (Supplementary Fig. 1). We also preferentially selected large minerals (when
359 possible) to limit the depth of each drill hole and the number of holes required to collect the
360 sufficient amount of material for Nd isotopic analysis. Finally, we carefully examined every
361 selected drilling area for fractures or inclusions and redefined the drilling area accordingly.
362
363 *LA-ICP-MS measurements and estimations of the Nd and Sr content of the sample*
364 We determined trace element concentrations on the selected clinopyroxenes and
365 plagioclases using laser ablation inductively coupled plasma mass spectroscopy (LA-ICP-MS).
366 Analyses were performed at Cardiff University on a New Wave research UP213 UV laser system
367 attached to a Thermo X Series 2 ICP-MS. Each mineral underwent two analyses (by lines) to allow
368 mineral compositional variability to be assessed. A minimum length of 300 μm and a beam
369 diameter of 80 μm were used, with a laser operating at 10 Hz frequency and sample translation at 6
370 μm s^{-1}. Acquisition time was about 80s (20s gas blank, >50 s acquisition, 10s washout)
371 We used the silicate glass standard NIST 612 as reference material, and clinopyroxene and
372 plagioclase Ca contents, measured by SEM-EDS, served as internal standard. We tested the
373 accuracy of the measurement with two external standards (BIR and BCR-2G) analyzed every 10
374 samples. Based on 10 BRC-2G measurements, the relative errors on the trace element contents lie
375 between 0.3 and 15%, with 3.8% and 5.2% for Nd and Sr respectively (Supplementary Fig. 3).
376
377 *Micro-sampling via Micro-mill*
378 Micromilling of the samples was performed in the Faculty of Sciences at Vrije Universiteit
379 Amsterdam (VUA) and in the School of Earth and Ocean Sciences at Cardiff University. We used a
380 procedure adapted from the that described by Charlier et al.[44] for thick sections. Polished billets
381 were first placed in an ultrasonic bath of Milli-Q water (standard purity with a final resistivity of
382 >18.4 MΩ) for 20 min, and then cleaned with acetic acid for one minute and finally cleaned and

dried with ethanol. Drill bits were also cleaned between each sampling in 0.165HCl for 2s and then in an ultrasonic bath of Milli-Q water for 10min.

We placed 2-3 drops of Milli-Q water on the area to be drilled. The drilled material is brought in suspension as the drilling proceeds. When the solution becomes saturated, it was pipetted into a Teflon vial previously cleaned for isotope chemistry and new drops of Milli-Q water were added to the drilling area. During the whole drilling procedure, we made sure that Milli-Q water was always present on the drilling area. Finally, at the end of the drilling sequence, all the water on the sample was collected.

After the micromilling was complete, we estimated the sampled volume by measuring the surface area and the depth of the hole. We also checked for the presence of inclusions. This gave us a maximum estimate of the volume of material collected, as not all the drilled material is recovered. Total procedural blanks were performed by simulating a 60min milling sequence on a clean sample. A clean drill bit was immersed into Milli-Q water on the rock slab sample, and the water was collected and resupplied following the same procedure than a regular micro-milling sequence in order to collect a similar amount of water. The blanks were then processed by column chemistry following the same procedure as the samples (see below).

Column chemistry

Separation of Sr and Nd from plagioclase and clinopyroxene cores

Column chemistry on plagioclase and clinopyroxene powders was performed at VUA and in the CELTIC laboratory at Cardiff University. Samples were dissolved in Teflon vials in a 4:1 mix of HF and HNO_3 on a hotplate at 140 °C for 3 days. Sr and rare earth elements (REEs) were separated from the matrix in a setup whereby Sr Resin columns (Eichrom, 50 µl resin) are placed directly above TRU Resin columns (Eichrom, 150 µl resin). By placing the Sr column above the TRU Resin column during loading and washing, the pre-fraction from the Sr Resin column (in 3 M HNO3) was directly eluted onto the TRU Resin column, after which the two column sets were

409 separated and Sr and REE were eluted. Finally, the Nd was further separated from the other REE in
410 a Ln-Resin column procedure (see Fig. 5 in Koornneef et al.[45] for details). Due to the large sample
411 size needed for Nd isotope analyses for plagioclase, most Sr plagioclase samples were subjected to
412 a second pass of Sr chemistry.
413 Total procedural blanks varied between 38 and 43 pg for Sr and 2 and 12 pg for Nd. The
414 blanks were determined by isotope dilution using an ^{84}Sr spike and a ^{150}Nd spike respectively.
415
416 *Separation of Sr and Nd on whole rock*
417 We performed whole rock (WR) isotopic analyses on six diabase samples, five
418 microgabbros and one olivine-rich troctolite from the core U1309D, as well as on eight basalts and
419 one basaltic glass recovered from IODP sites U1310 and U1311 (see Supplementary Figure 1 for
420 locations of the drill cores). Column chemistry was performed in the CELTIC laboratory at Cardiff
421 University. Samples were crushed into an agate ball mill grinder and we collected between 200 and
422 300 mg . All but the glass sample (1310-A1-13-19) were leached in hot 6 M HCl for 3 h and then
423 rinsed to remove unbonded Sr[46]. The glass powder was leached at room temperature in 6 M HCl for
424 30 min. After centrifugation of the samples, the supernatant was discarded and samples were
425 washed in MQ, centrifuged again and the supernatant was again discarded. Residual powders were
426 then digested in hot concentrated HNO_3 and HF for 24 h, dried down, taken up in 1 mL of
427 concentrated HNO_3 and dried down again before being redissolved in 8 M HNO_3, and centrifuged.
428 Sr was separated in a double pass through a 1 mL pipette-tip column containing Sr-spec
429 resin. Samples were loaded in 8 M HNO_3 and sample matrix (including Ca and Rb) was removed in
430 the same acid. Sr was then collected in 0.05M HNO_3[47]. Samples were dried again and sequentially
431 brought into solution in concentrated HNO_3 and HCl, refluxed on a hotplate for at least 24 h, and
432 finally dried down prior to being brought into solution in dilute HCl.

Nd was separated in two steps. The REE were first separated from the sample matrix using columns filled with a cation exchange resin (BioRad AG50W-x8, 2.5 mL). The REE fraction was then dried and Nd was separated using columns filled with Ln-Spec resin (Eichrom, 1.1 mL)[48]. Total procedural blanks were 10 and 15 pg for Sr and Nd, respectively.

Mass spectrometry

Clinopyroxene and plagioclase samples

Sr and Nd analyses on plagioclase and clinopyroxene cores were performed on a Thermo Scientific Triton-Plus TIMS at VUA. Samples and standards were loaded on outgassed Re filaments in a clean air flow unit. Strontium analyses were performed using annealed Re filaments in a single filament set-up whereas for Nd analyses annealed and zone-refined Re filaments were used in a double filament configuration for the evaporation and ionisation positions, respectively[45,49]. Isotope analyses were performed using 10^{11} Ω amplifiers in the feedback loop of the Faraday detectors. Six of the current amplifiers installed in the TRITON Plus at VU Amsterdam have the conventional 10^{11} ohm resistors, whereas the other 4 amplifiers are equipped with 10^{13} ohm resistors. The Sr and Nd collection measurements reported here were carried out using the same static analytical approach as Koornneef et al.[49].

The estimated amount of Nd and Sr analyzed, as well as the number of cycles for each analysis, are reported in Supplementary Table 1. An 11 min baseline was measured during heating of the sample and subtracted online from the raw intensity values. In most cases, analyses were run to exhaustion. On average, we acquired 194 and 214 cycles for Sr isotopic analyses in plagioclase and clinopyroxenes, respectively, and 85 and 97 cycles for Nd isotopic analyses in plagioclase and clinopyroxene, respectively.

The intensities on the 87 Mass are corrected for minor ^{87}Rb contributions by using the canonical $^{87}Rb/^{85}Rb$ of 0.3857. Sm was not detected for all but three clinopyroxenes (149R2-68-71a, 252R4-3-6a and 257R1-95-100a). For the three clinopyroxenes where we detected ^{147}Sm we

459 correct the 144 intensity using $^{144}Sm/^{147}Sm = 0.20502$. Nd and Sr measurements are subsequently
460 corrected for instrumental mass fractionation by using the exponential law, and $^{146}Nd/^{144}Nd =$
461 0.7219 and $^{86}Sr/^{88}Sr = 0.1194$, respectively. To test the accuracy of the measurements, 7-8 mg of
462 BHVO-2 standards were passed through the complete chemical procedure. Filaments were loaded
463 with either 2 or 10 ng of Nd, and with 200ng of Sr. Data are within the error of the preferred values
464 reported in GeoReM database (Supplementary Fig. 4).
465
466 *Whole rock*
467 Sr and Nd isotope ratios were measured on a Nu Instruments multi-collector (MC)-ICP-MS
468 system in the CELTIC laboratory at Cardiff University in static mode. Sr isotopic measurements
469 were normalized internally to $^{86}Sr/^{88}Sr = 0.1194$ and NBS-987 was run every five samples as a
470 secondary correction to account for small variations in non exponential mass bias. ^{86}Kr
471 interferences were below background level, therefore no correction was made. Nd isotopic
472 measurements were normalized internally to $^{146}Nd/^{144}Nd = 0.7219$ and JNd-i was run every five
473 samples a secondary correction to account for small variations in non exponential mass bias.
474 Accuracy of the measurements was tested using JB-2 as a secondary standard that was passed
475 through the complete chemical procedure and the Sr and Nd isotopic ratios obtained are
476 indistinguishable within error from the preferred values reported in GeoReM database
477 (Supplementary Fig. 5).
478
479 *Calculation of the contribution of the recycled material to the parental melts and fraction of*
480 *recycled material-derived melt in parental melts*
481 For the enriched component, we used the isotopic ratio of the most enriched clinopyroxene analysed
482 in this study ($^{143}Nd/^{144}Nd = 0.512800 \pm 15$; $^{87}Sr/^{86}Sr = 0.702884 \pm 9$). Such isotopic signature can
483 be reproduced by partial melting of a ~ 1.1 Ga recycled gabbro[50] (Supplementary Fig. 2). We used
484 the same major and trace element composition used to calculate the age, i.e. the average oceanic

485 gabbro composition estimated by Hart et al.[24]. For the depleted component, we used the isotopic
486 ratio of the most depleted abyssal peridotite reported along the MAR (Vema lithospheric section[7],
487 $^{143}Nd/^{144}Nd = 0.51366$) and major and trace element compositions of the depleted endmember of
488 the depleted MORB mantle (D-DMM[51]). To estimate the fractions of each end-member in the
489 parental melts of cumulate minerals, we need to know the Nd content of melt generated by each
490 end-member. Following the approach used by Lambart et al.[22], we considered that the mantle
491 follows an adiabatic path, with a potential temperature of T_P = 1300°C. Both components are in
492 thermal equilibrium and chemically isolated. We used Melt-PX[52] to calculate the Pressure (P) –
493 Temperature (T) - Melt fraction (F) path. We considered that both lithologies were chemically
494 isolated but in thermal equilibrium. Calculations performed with Melt-PX take into account heat
495 transfer between the different lithologies. Calculations were stopped when the mantle column had
496 upwelled to the base of the crust, i.e. when the pressure at the base of the crust, $P_c = P$. The initial
497 fraction of recycled gabbro in the mantle source (i.e., 5%) was chosen such that a 5-6 km crust
498 thickness was generated[29]. We used alphaMELTS[53] to calculate the mineral assemblage at each
499 pressure step (i.e., every 100 bars) for each lithology. We calculated the Nd content of the melt
500 derived from each lithology along the adiabatic path using incremental batch melting calculations,
501 integrating the liquid produced over the melting region and dividing by the total volume produced
502 (see Lambart[22] for details on calculations). Accumulated Nd content of the melt derived from the
503 recycled crust ($[Nd]_{RC}$) and DDMM ($[Nd]_{DDMM}$) are 8.1 and 2.7ppm, respectively. We can solve for
504 the fraction of recycled crust (F_{RC}) required to explain the isotopic mineral compositions such as:
505 $$^{143}Nd/^{144}Nd_{cpx/plag} = (F_{RC} \times [Nd]_{RC})/(F_{RC} \times [Nd]_{RC} + (1- F_{RC}) \times [Nd]_{DDMM}) \times {}^{143}Nd/^{144}Nd_{RC} +$$
506 $$(1 - (F_{RC} \times [Nd]_{RC})/(F_{RC} \times [Nd]_{RC} + (1 - F_{RC}) \times [Nd]_{DDMM})) \times {}^{143}Nd/^{144}Nd_{DDMM}$$
507
508 *Nature of the enriched component.*
509 As noted above, we assumed that the lowest $^{143}Nd/^{144}Nd$ ratio is produced by partial melting of a ~
510 1.1 Ga recycled gabbro[50]. However, other processes can produced similar isotopic ratios, such as a

511 small contribution of recycled sediments[50] or the partial melting of hybrid lithologies resulting from
512 the mixture between older recycled material and peridotite. Contribution of sediments is
513 accompanied by strong enrichments in $^{87}Sr/^{86}Sr$ and $^{176}Hf/^{177}Hf$, which are difficult to reconcile
514 with the observed MORB array[50]. To investigate the effect of the nature of the enriched material on
515 our calculations, we performed an additional set of calculations using a hybrid lithology, produced
516 by a 1:1 mix between recycled gabbro and depleted peridotite. We used KG1[54] for the major
517 elelemt composition and calculated trace elelement composition as a 1:1 mixture between the
518 oceanic gabbro[24] and D-DMM[51]. The most enriched clinopyroxene Nd isotopic ratio can be
519 reproduced assuming the recycled gabbro is ~1.3 Ga[50]. The calculated Nd content of the
520 accumulated melt derived from KG1 is 3.8ppm. Solving for the fraction of KG1 in the melt, we
521 obtained significantly higher (48 to 75%) contribution of KG1-derived melt in the aggregated
522 magma. Using the estimated fraction of KG1 in the melt, we calculated the corresponding fraction
523 in the source. We can then estimate the proportion of recycled crust in the mantle simply using the
524 relationship $X_{RC}^{source} = 0.5\ X_{KG1}^{source}$. Both calculations produce similar profiles of thickness
525 variation (Supplementary Fig. 6c). However, for T_P = 1300°C, calculations using KG1 yield to a
526 proportion of recycled crust between 9 and 21% (Supplementary Fig. 6e). These estimations are
527 significantly higher than previous estimation for the amount of recycled crust in the mantle source
528 of MORB[55,56]. In summary, the enriched signature can reflect either the direct participation of
529 crustal material (i.e., by partial melting) or its indirect participation, by interaction with the
530 surrounding peridotite and subsequent melting of an "enriched" peridotite/hybrid lithology.
531 However, because of the higher solidus temperatures of peridotite or hybrid lithology such as KG1
532 in comparison to the recylced crust[51], the proportion of enriched material in the mantle required to
533 reproduce the enriched melt composition is significantly higher in the latter case, resulting to a
534 higher initial proportion of recycled crust needed to produce this enriched composition.
535
536 *Condition for the preservation of the mantle component isotopic signatures.*

The recycled crust has a higher melt productivity[52] and Nd abundance[24] than the peridotite[51]. Hence, even a small degree of mixing will dilute the signature of the most depleted component. Inversely a small contribution of depleted peridotite melt to the recycled crust-derived melt will not significantly affect the isotopic composition of the latter, and aggregated melts are more likely to sample the enriched end-member composition. In fact, 14% of recycled crust-derived melt in the aggregated magma is required to change the Nd isotopic ratio of the melt from 0.51366 to 0.51332 (i.e, from the most depleted abyssal peridotite[7] to the most depleted cumulate mineral). However, a 14% addition of peridotite melt to the recycled crust-derived melt would only change its isotopic ratio from 0.51280 to 0.51283 (i.e, unchanged within error). Hence, while the isotopic composition of the depleted end-member is most likely to be diluted, the most enriched composition observed in cumulate minerals is a good representative of the enriched end-member in the mantle beneath the Atlantis massif.

Code availability. The code used to calculate adiabatic melting of a two component mantle source, Melt-PX[52], can be accessed at https://doi.org/10.1002/2015JB012762 .

Data availability. The authors declare that data supporting the findings of this study are available within the paper, the Methods and in the PetDB data repository (http://www.earthchem.org/petdbWeb/search/readydata/MAR55S-52N_major_trace_isotope.csv).

References

44. Charlier, B. L. A. et al. Methods for the microsampling and high-precision analysis of strontium and rubidium isotopes at single crystal scale for petrological and geochronological applications. *Chem. Geol.* 232, 114-133 (2006).

45. Koornneef, J. M. et al. TIMS analysis of Sr and Nd isotopes in melt inclusions from Italian potassium-rich lavas using prototype 10^{13} Ω amplifiers. *Chem. Geol.* 397, 14-23 (2015).

563 46. Millet, M. –A., Doucelance, R., Schiano, P., David, K., Bosq, C. Mantle plume heterogeneity
564 versus shallow-level interactions: A case study, the São Nicolau Island, Cape Verde
565 archipelago. *J. Volcanol. Geotherm. Res.* 176, 265–276 (2008).
566 47. McGee, L. E., Smith, I. E., Millet, M. -A., Handley, H. K., Lindsay, J. M. Asthenospheric
567 control of melting processes in a monogenetic basaltic system: A case study of the Auckland
568 Volcanic Field, New Zealand. *J. Petrol.* 54(10), 2125-2153 (2013).
569 48. McCoy-West, A. J., Millet, M. -A., Burton, K. W. The neodymium stable isotope composition
570 of the silicate Earth and chondrites. *Earth Planet. Sci. Lett.* 480, 121-132 (2017).
571 49. Koornneef, J. M., Bouman, C., Schwieters, J. B., Davies, G. R. Use of 10^{12} ohm current
572 amplifiers in Sr and Nd isotope analyses by TIMS for application to sub-nanogram samples. *J.*
573 *Anal. At. Spectrom.* 28, 749-754 (2013).
574 50. Stracke, A., Bizimis, M., Salters, V. J. M. Recycling oceanic crust: Quantitative constraints.
575 *Geochem. Geophys. Geosyst.* 4(3), 8003 (2003).
576 51. Workman, R. K., Hart, S. R. Major and trace element composition of the depleted MORB
577 mantle (DMM). *Earth Planet. Sci. Lett.* 231, 53–72 (2005).
578 52. Lambart, S., Baker, M. B., Stolper, E. M. The role of pyroxenite in basalt genesis: Melt-PX, a
579 melting parameterization for mantle pyroxenites between 0.9 and 5GPa. *J. Geophys. Res. Solid*
580 *Earth* 121, 5708–5735 (2016).
581 53. Smith, P.M., Asimow, P.D. Adiabat_1ph: A new public front-end to the MELTS, pMELTS, and
582 pHMELTS models. *Geochem. Geophys. Geosyst.* 6, Q02004 (2005).
583 54. Kogiso, T., Hirose, K., Takahashi, E. Melting experiments on homogeneous mixtures of
584 peridotite and basalt: application to the genesis of ocean island basalts. *Earth Planet. Sci. Lett.*
585 162, 45-61 (1998).
586 55. Hirschmann, M. M., Stolper, E.M. A possible role for garnet pyroxenite in the origin of the
587 “garnet signature” in MORB. *Contrib. Mineral. Petrol.* 124, 185-208 (1996).

588 56. Sobolev, A.V. et al. The amount of recycled crust in sources of mantle derived melts. *Science*
589 316, 590–597 (2007).

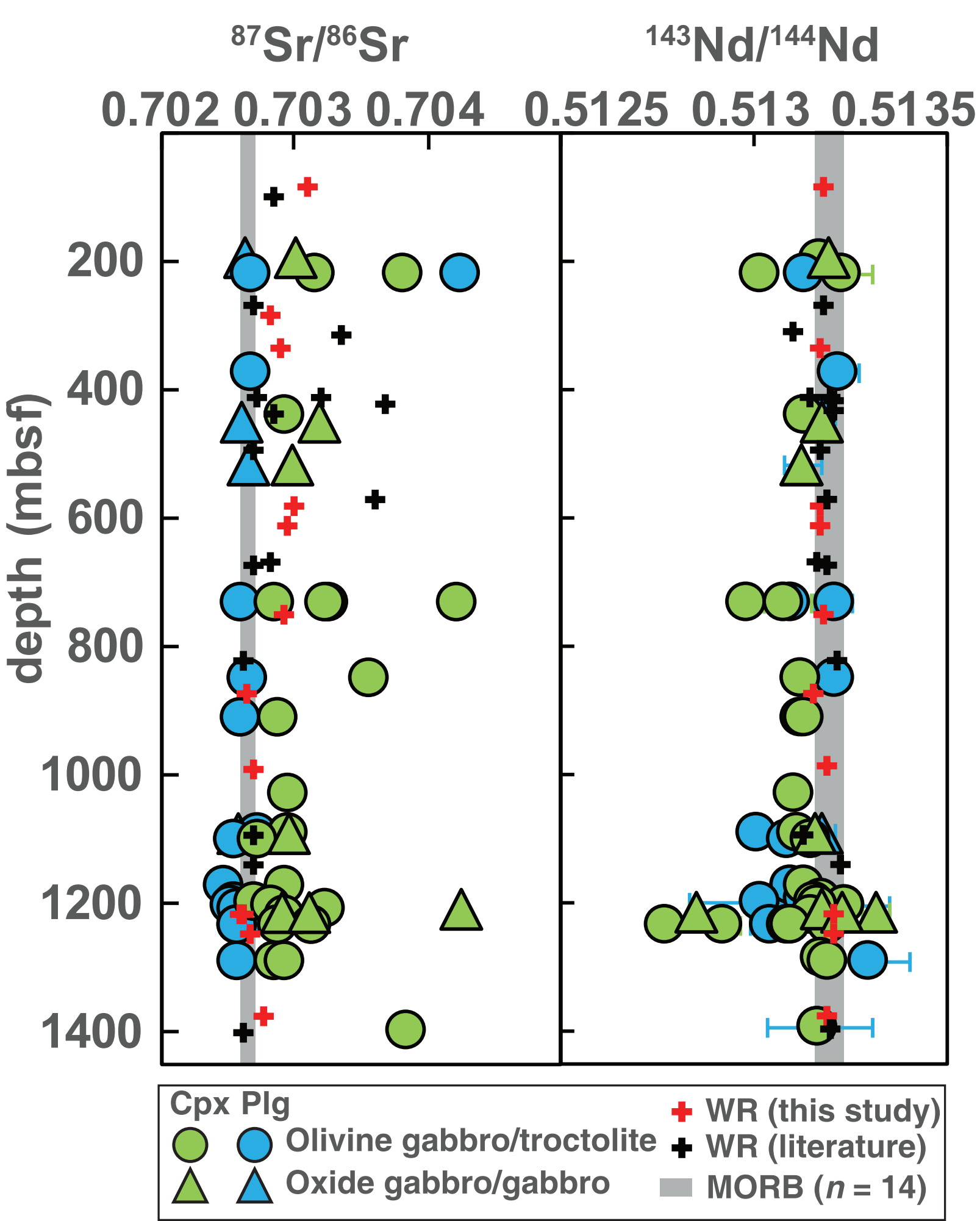
$^{87}Sr/^{86}Sr$
$^{143}Nd/^{144}Nd$
0.702
0.703
0.704
0.5125
0.513
0.5135
depth (mbsf)
200
400
600
800
1000
1200
1400
Cpx Plg
Olivine gabbro/troctolite
Oxide gabbro/gabbro
WR (this study)
WR (literature)
MORB (n = 14)

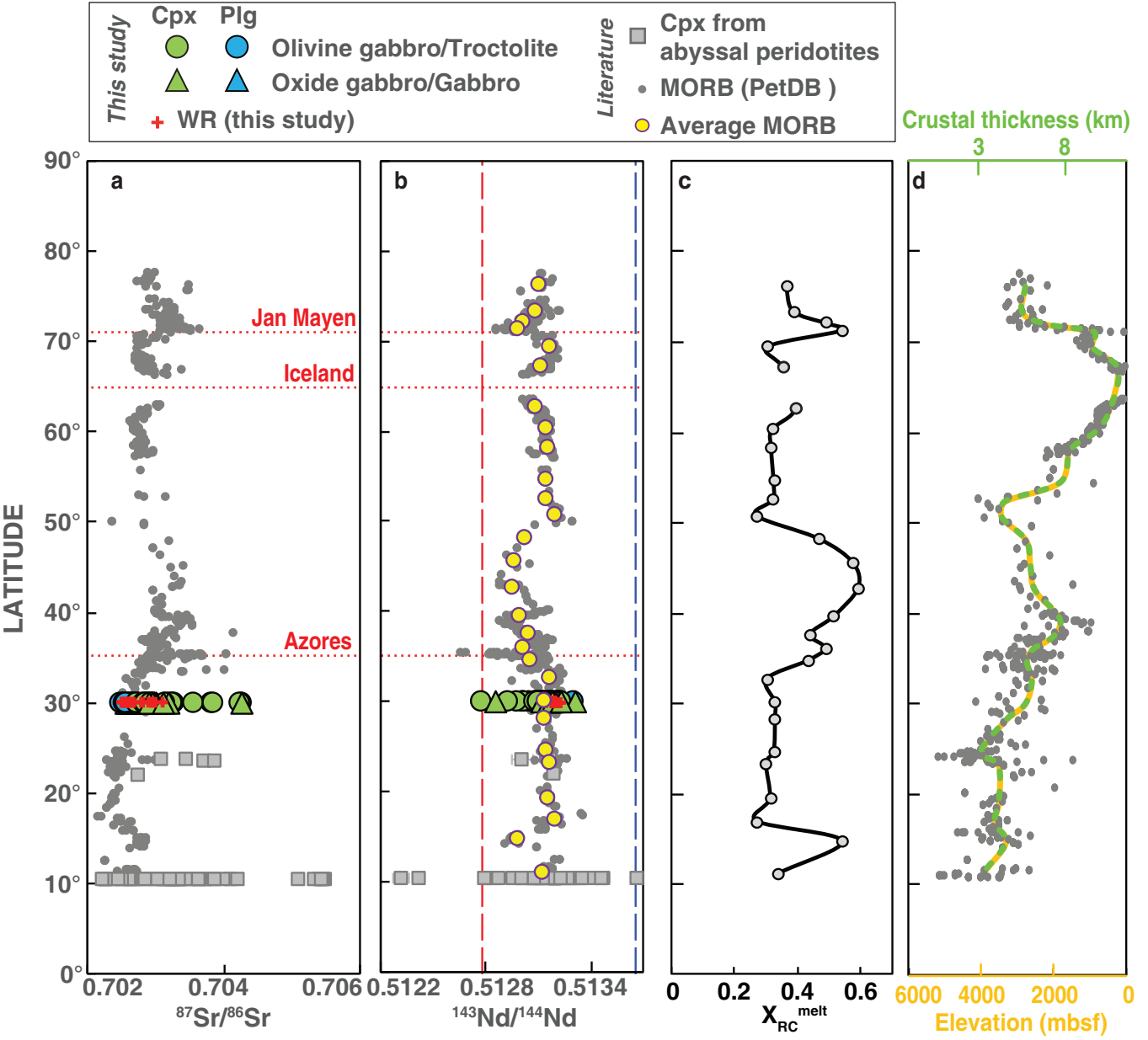
This study
Cpx
Plg
Olivine gabbro/Troctolite
Oxide gabbro/Gabbro
WR (this study)
Literature
Cpx from abyssal peridotites
MORB (PetDB)
Average MORB
Crustal thickness (km)
3
8
a
b
c
d
Jan Mayen
Iceland
Azores
LATITUDE
90°
80°
70°
60°
50°
40°
30°
20°
10°
0°
0.702
0.704
0.706
87Sr/86Sr
0.5122
0.5128
0.5134
143Nd/144Nd
0
0.2
0.4
0.6
XRCmelt
6000
4000
2000
0
Elevation (mbsf)

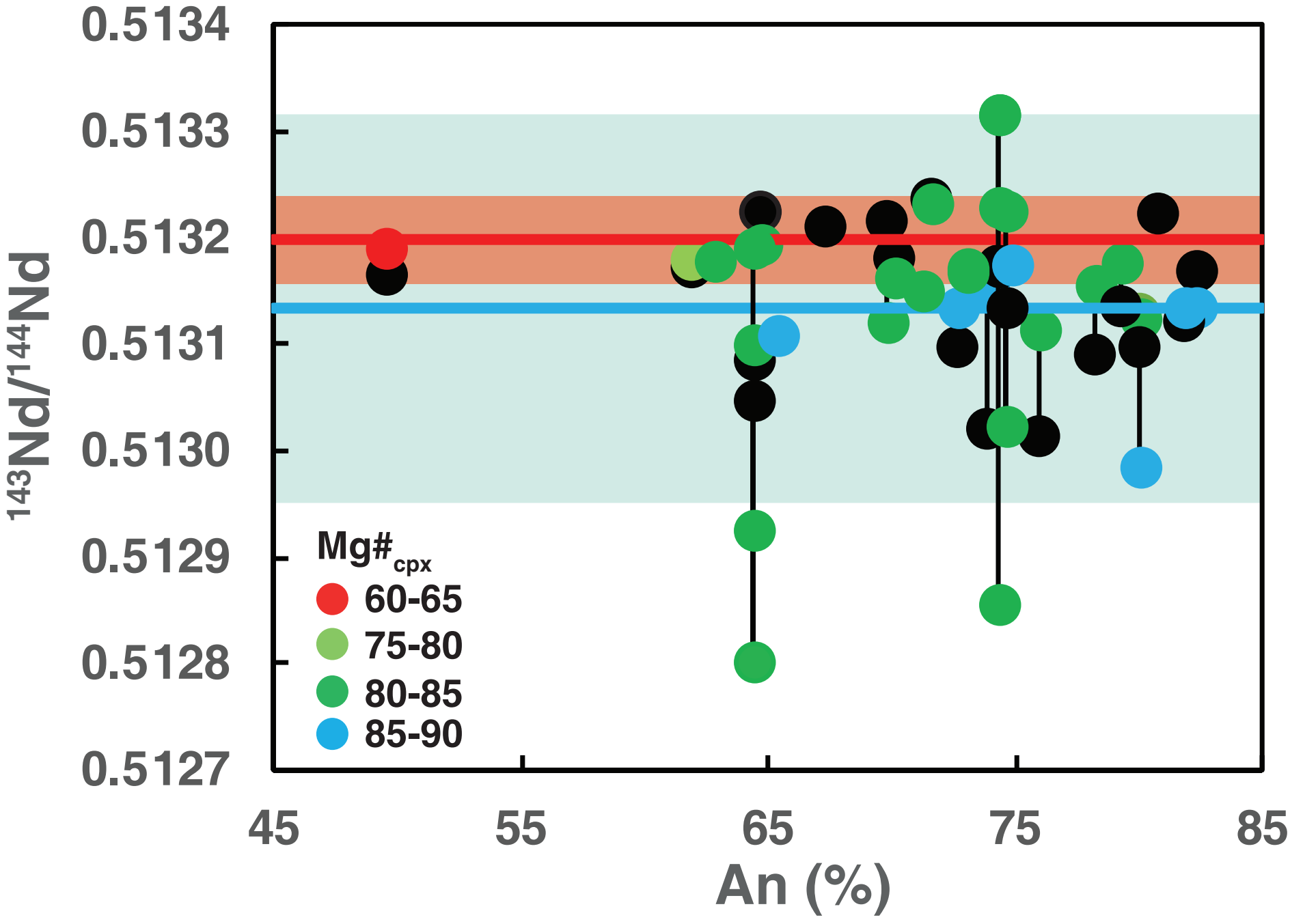
0.5134
0.5133
0.5132
0.5131
0.5130
0.5129
0.5128
0.5127
143Nd/144Nd
45
55
65
75
85
An (%)
Mg#cpx
60-65
75-80
80-85
85-90

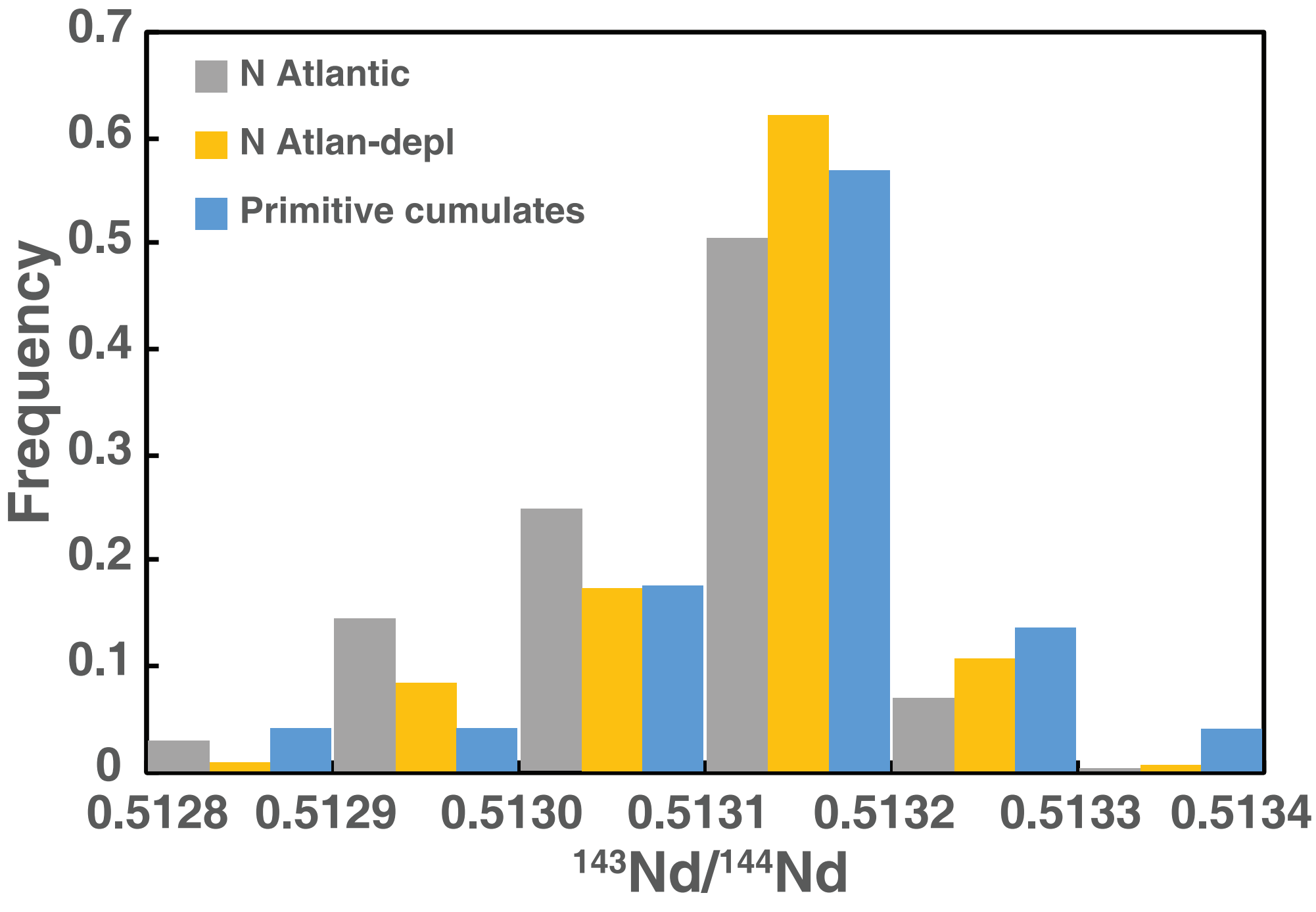
N Atlantic
N Atlan-depl
Primitive cumulates
Frequency
0.7
0.6
0.5
0.4
0.3
0.2
0.1
0
0.5128
0.5129
0.5130
0.5131
0.5132
0.5133
0.5134
143Nd/144Nd

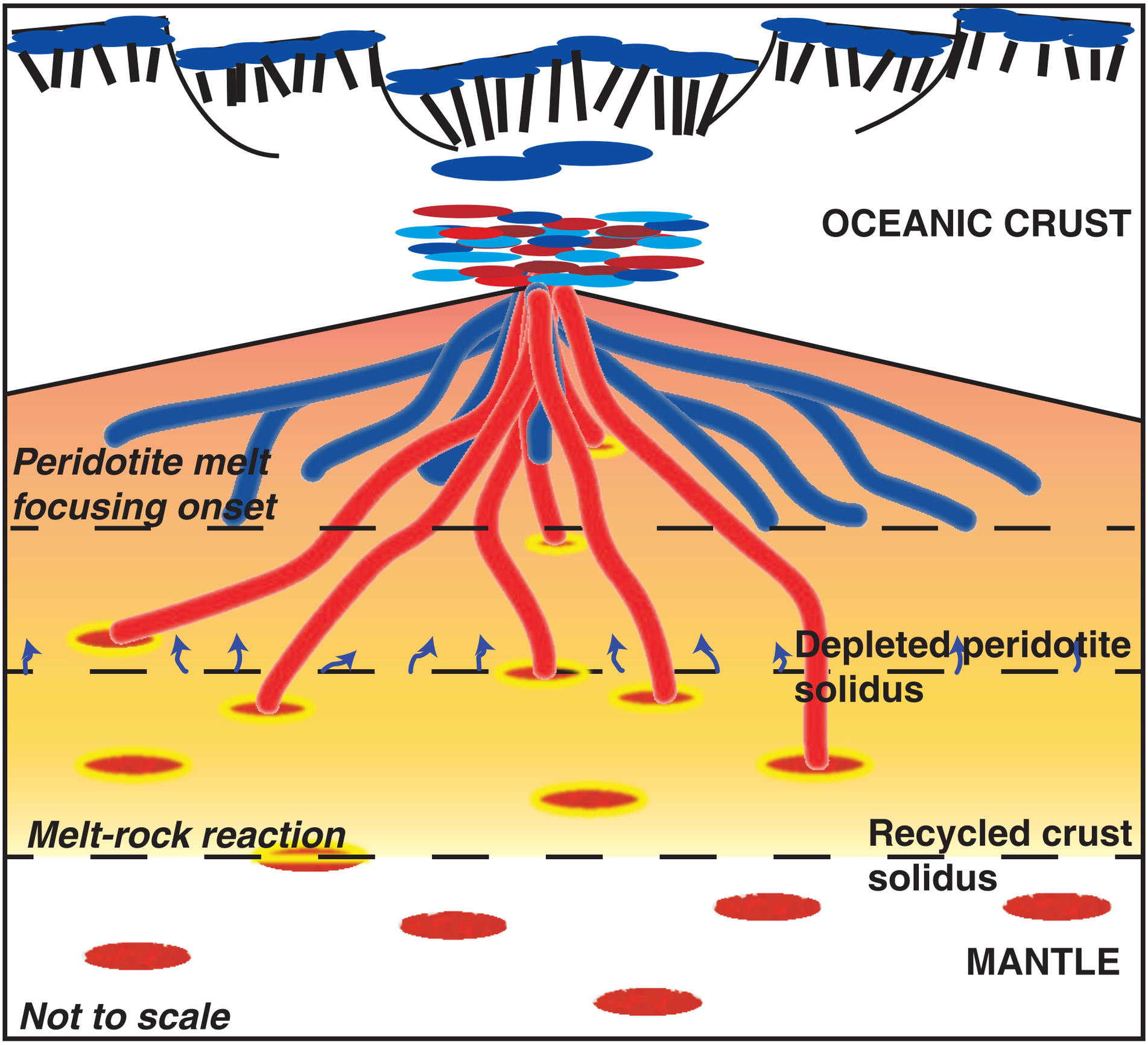
OCEANIC CRUST
Peridotite melt
focusing onset
Depleted peridotite
solidus
Melt-rock reaction
Recycled crust
solidus
MANTLE
Not to scale

Supplementary Figures and Table to accompany 'Highly Heterogeneous Depleted Mantle Recorded in the Lower Oceanic Crust' by Lambart et al.

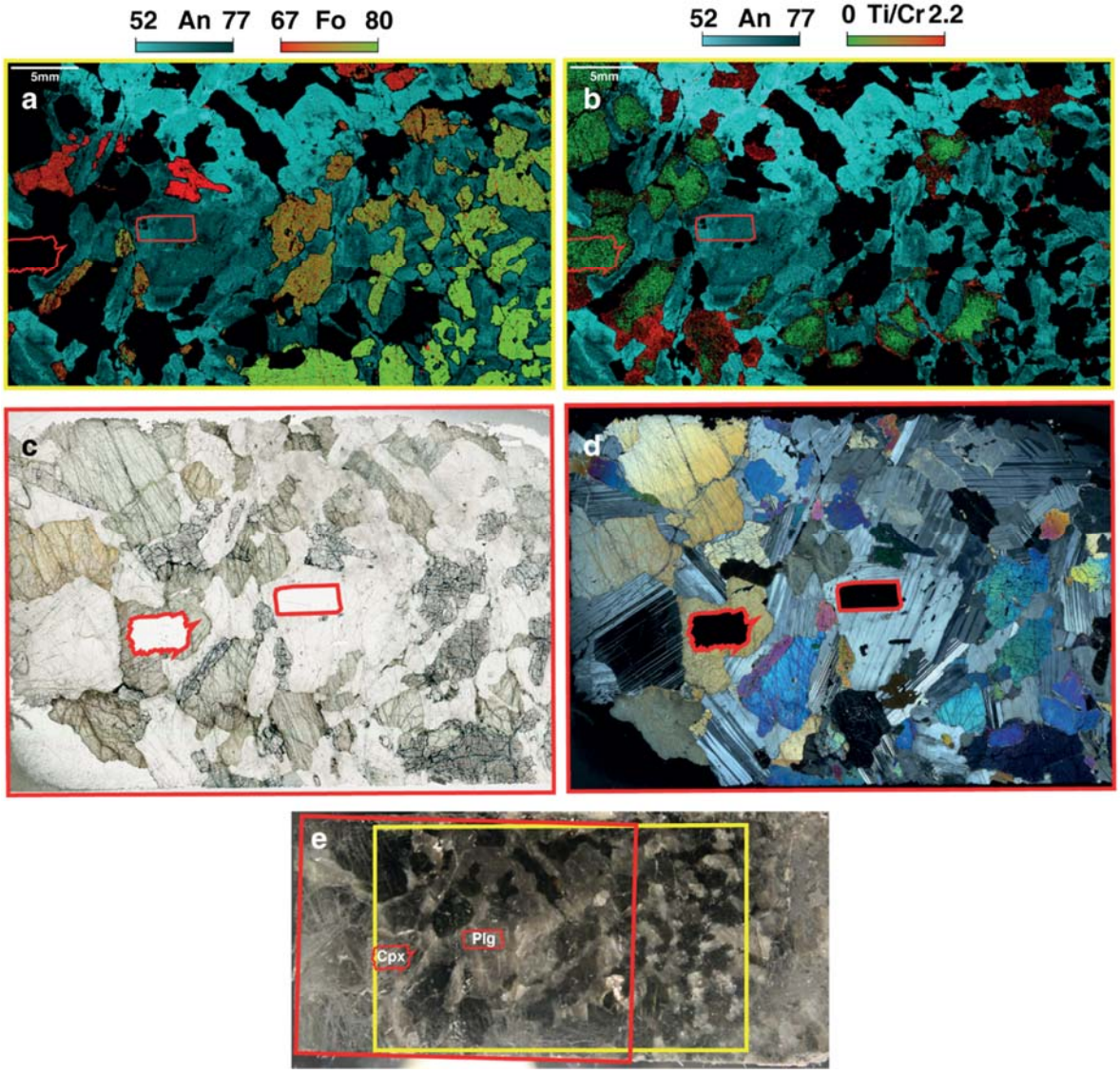

Supplementary Figure 1. Illustration of the method for selecting micro-milling sites. Mg–Fe–Na **(a)** and Ti-Cr-Na **(b)** element maps, photomicrographs **(c-d)** showing the microdrill locations, and core photo **(e)** showing the element map area (yellow), the thin section area (red) of the olivine gabbro 268R3-6-12 from IODP Hole U1309D. Map (a) shows Fo (red to green) and An (light to dark blue) content variations of olivine and plagioclase at the scale of the sample. Clinopyroxene appears black because Fe and Mg have been scaled to show the olivine compositions. Map (b) highlight An content of plagioclase and TiO_2/Cr_2O_3 ratio in clinopyroxene. Red highlighted area indicate microdrill location. A noteworthy feature is the substantial An, Fo and TiO_2/Cr_2O_3 variations on a cm scale (a-b).

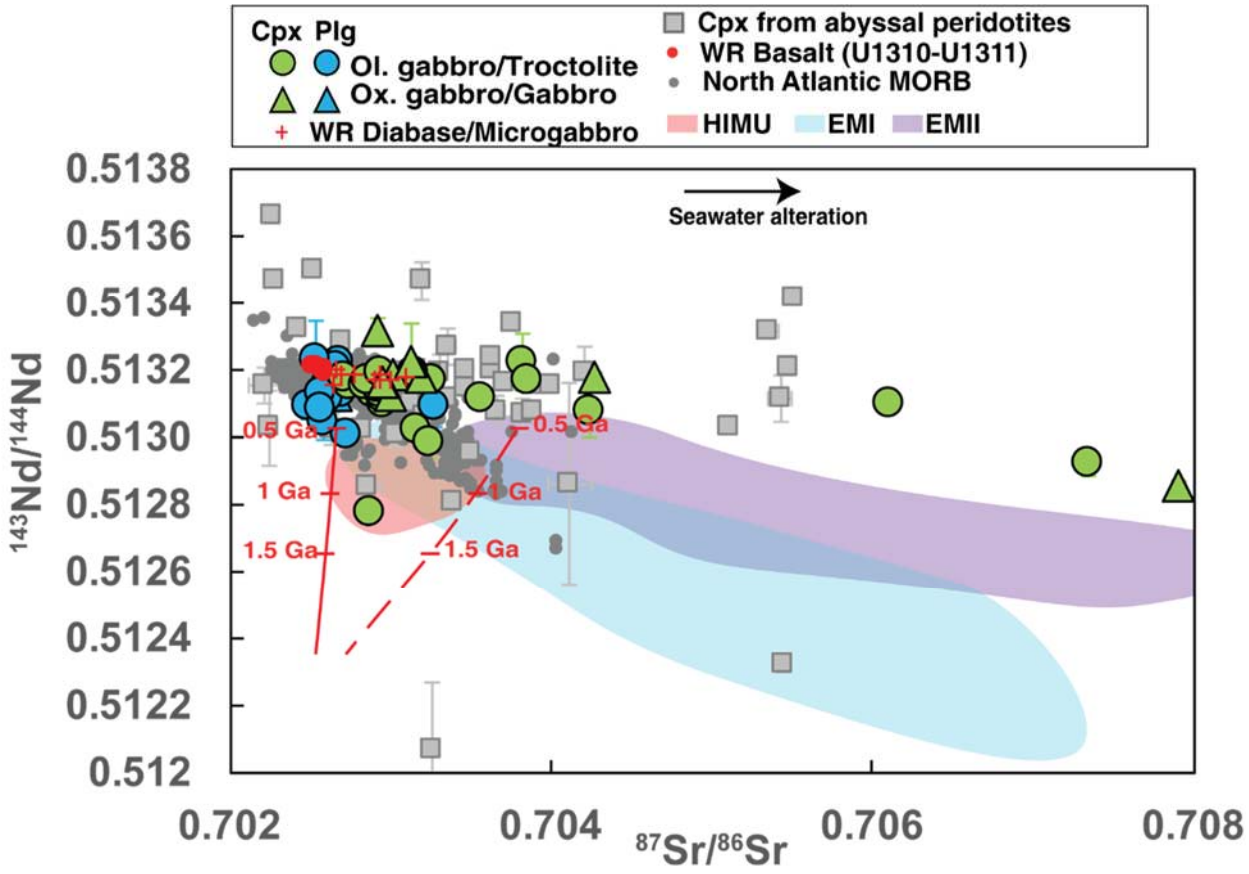

Supplementary Figure 2. Comparison between isotopic compositions analysed in this study and compositions of North Atlantic MORB. $^{143}Nd/^{144}Nd$ versus $^{87}Sr/^{86}Sr$ ratios of Atlantis Massif clinopyroxene and plagioclase compared with whole rock (WR) diabase and basalt isotopic analyses performed in this study, theNorth Atlantic MORB compositions reported in the literature (PetDB database[42]) and the clinopyroxene compositions from abyssal peridotites collected along the MAR[7,12,13]. Compositional fields of HIMU (red), EMI (blue) and EMII (purple) basalts are shown for comparison[50]. The red lines are calculated present-day isotopic compositions of recycled oceanic gabbro affected (dashed line) or not (solid line) by seawater alteration, as a function of recycling age[50]. Error bars: 2SEE.

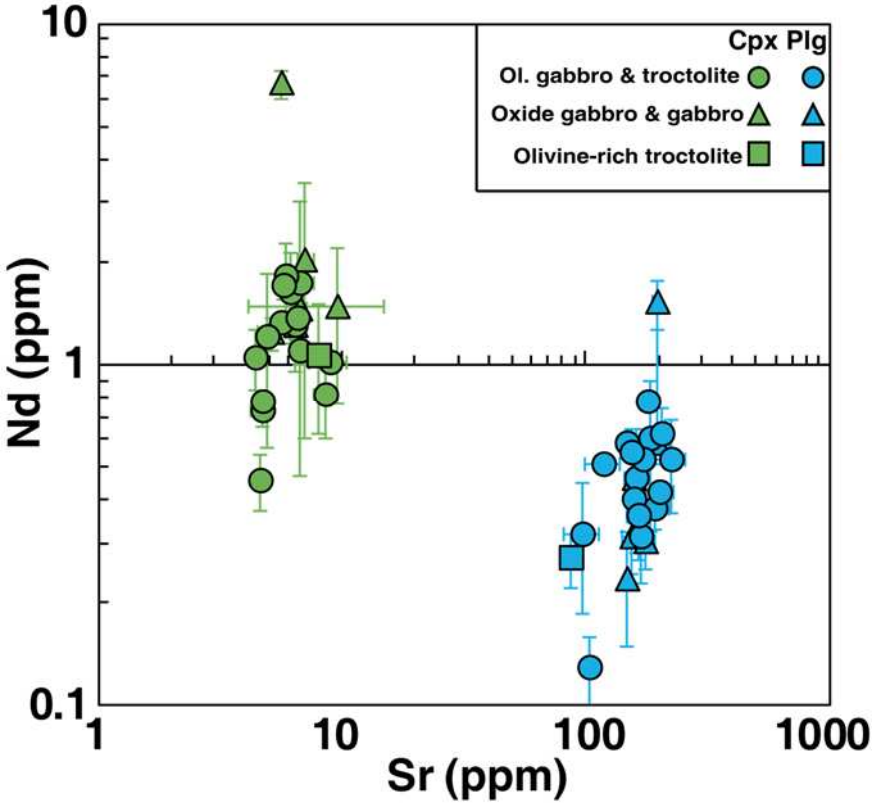

Supplementary Figure 3. Sr and Nd concentrations in selected minerals for micromilling (2σ error bars).

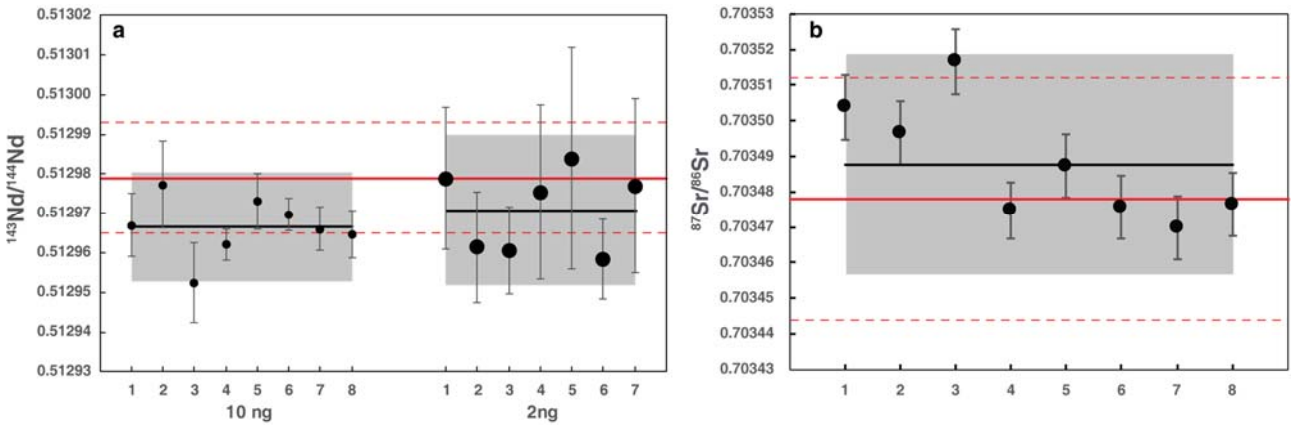

Supplementary Figure 4. Standard analyses on TIMS. a. $^{143}Nd/^{144}Nd$ ratios (2SE error bars) measured on BHVO-2. Filaments were loaded with 10 ng (small circles) or 2 ng of Nd (large circles). **b.** $^{87}Sr/^{86}Sr$ ratios (2SE error bars) measured on 200ng Sr separated from BHVO-2. Black line and grey band are the average and 2SD measured on BHVO-2 in this study. Solid and dashed red lines are average and 2SD reported for BHVO-2 in GeoReM database.

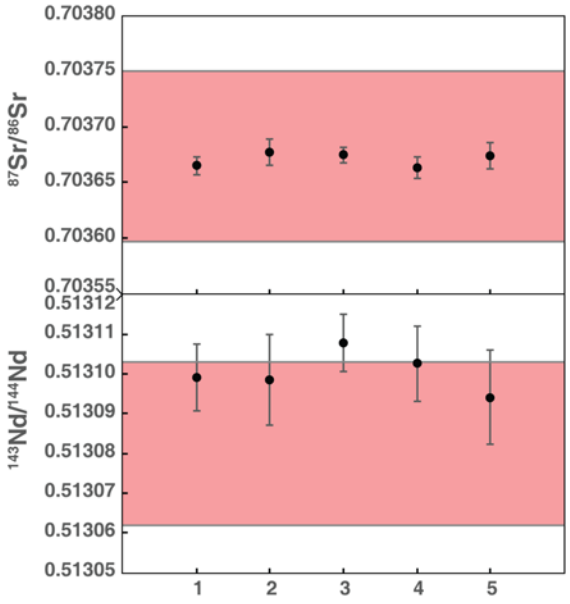

Supplementary Figure 5. Standard analyses on Nu Instrument. $^{87}Sr/^{86}Sr$ and $^{143}Nd/^{144}Nd$ ratios measured on JB-2 after correction for fractionation and mass bias (2SE error bars). Red bands are the range of values reported for JB-2 in GeoReM database.

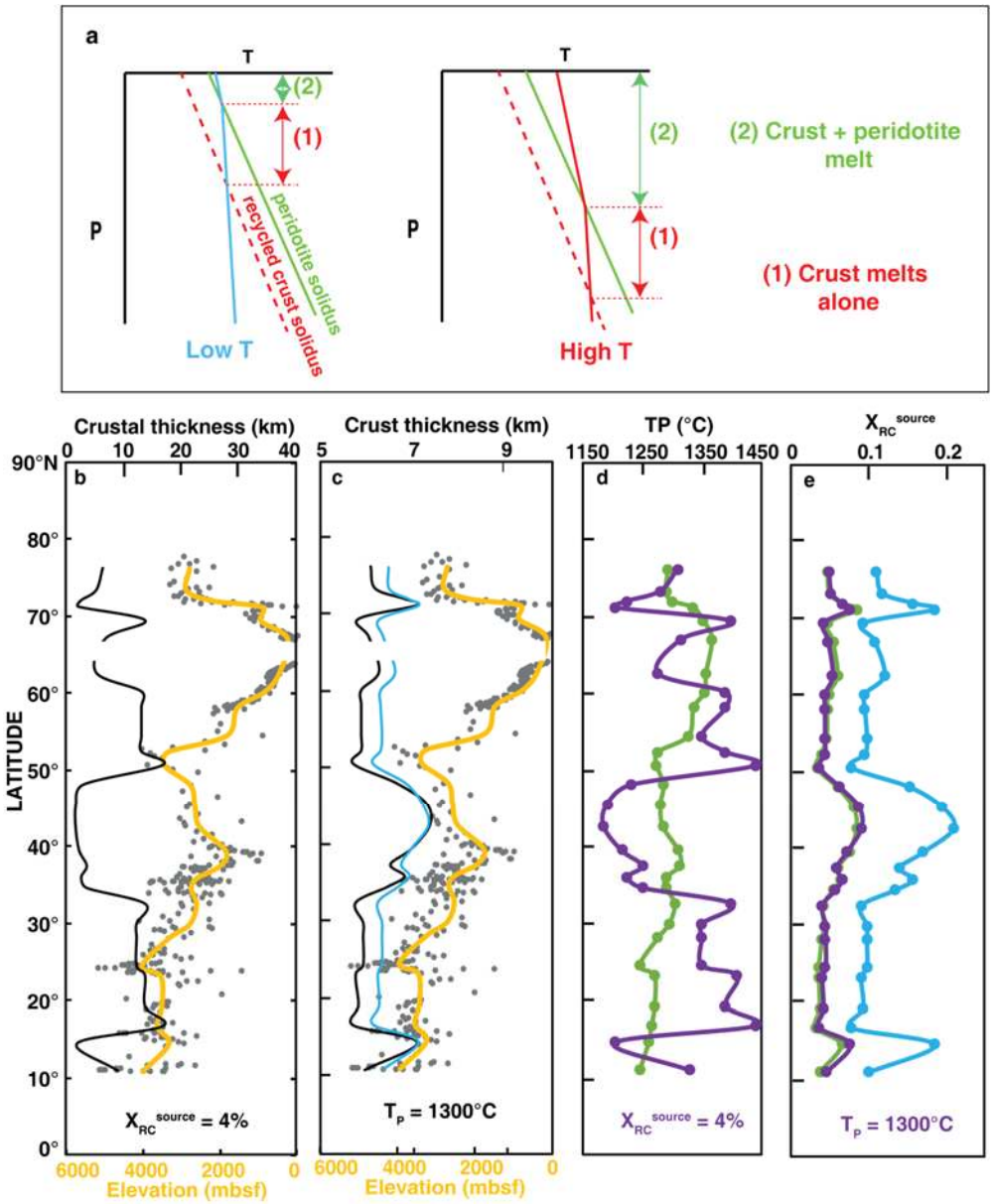

Supplementary Figure 6. Results of geochemical modelling. a. Schematic illustration of the effect of mantle potential temperature (T_P) on the fraction of recycled crust in the melt: increasing T_P decreases the ratio between the interval where only the recycled crust is melting and the interval where both crust and peridotite are melting (i.e., (1)/(2) ratio). **b-c**. Comparison between the average MORB elevations (orange line) with the calculated crust thicknesses (black line), assuming a constant fraction of recycled crust, X_{RC} = 4%, and varying T_P (b), or assuming a constant T_P = 1300°C and varying the proportion of recycled crust (c). **d.** Calculated T_P with constant X_{RC} = 4% (purple) and the hybrid model (green). **e.** Calculated X_{RC}^{source} with constant T_P = 1300°C (purple) and with the hybrid model (green). In (c) and (e), the blue line shows the results using T_P = 1300°C and the composition KG1 for the enriched material.

Supplementary Table 1. Isotopic analyses of clinopyroxenes, plagioclase and whole rocks plotted in Figs. 1&2.

Sample	depth	Plagioclase						Clinopyroxene						Whole rock	
	(mbsf)	$^{87}Sr/^{86}Sr$	Sr*	*n*	$^{143}Nd/^{144}Nd$	Nd*	*n*	$^{87}Sr/^{86}Sr$	Sr*	*n*	$^{143}Nd/^{144}Nd$	Nd*	*n*	$^{87}Sr/^{86}Sr$	$^{143}Nd/^{144}Nd$
15R1-43-45	84.54													0.703096 (9)	0.513184 (8)
36R1-48-53	196.09	0.702643 (8)	200	185	0.513169 (30)	8	114	0.703023 (10)	35	208	0.513191 (9)	30	168		
41R2-27-31a	221.25	0.702693 (8)	200	200	0.513136 (20)	2	96	0.703158 (14)	50	212	0.513024 (16)	4	181		
41R2-27-31b	221.50	0.704276 (44)	200	95				0.703823 (36)	50	54	0.513226 (87)	5	54		
54R3-125-126	285.15													0.702825 (10)	
65R1-141-143	335.42													0.702905 (11)	0.513169 (11)
73R2-124-129	375.12	0.702675 (9)	150	200	0.513224 (45)	3	59								
88R4-110-113	443.07				0.513170 (40)	1	66	0.702941 (9)	15	259	0.513135 (16)	3	82		
90R3-22-27	451.85	0.702600 (8)	200	200	0.513175 (24)	2	93	0.703196 (36)	120	501	0.513179 (3)	30	203		
104R3-113-115	519.76	0.702660 (9)	200	200	0.513127 (46)	2	77	0.703000 (8)	30	240	0.513125 (12)	8	80		
117R3-86-87	581.70													0.702999 (8)	0.513170 (8)
125R2-119-121	614.06													0.702941 (9)	0.513171 (10)
149R2-16-21	733.49	0.702611 (26)	200	200	0.513213 (40)	5	95	0.702861 (13)	30	208	0.513180 (72)	15	125		
149R2-68-71a	734.00	0.703272 (10)	200	200	0.513096 (64)	2	55	0.703238 (10)	15	222	0.512986^{+} (41)	2	94		
149R2-68-71b	734.00							0.704235 (57)	27	110	0.513078 (77)	5	56		
153R1-25-24	751.25													0.702938 (8)	0.513186 (8)
175R2-25-28	853.00	0.702662 (25)	200	100	0.513214 (34)	1	132	0.703571 (14)	50	272	0.513121 (18)	5	98		
179R4-118-123	875.33													0.702644 (7)	0.513154 (9)
187R3-23-27	911.63	0.702611 (8)	200	200	0.513121 (34)	6	74	0.702893 (9)	40	224	0.513135 (23)	10	80		
205R4-63-66	990.38													0.702698 (8)	0.513190 (9)
214R1-138-143	1031.01							0.702961 (10)	25	201	0.513106 (10)	5	139		
227R1-112-117	1093.15	0.702575 (8)	250	200	0.513179 (36)	2	76	0.702963 (10)	25	219	0.513163 (23)	5	86		
227R2-28-33	1093.74	0.702732 (8)	200	189	0.513012 (33)	3	108	0.702959 (10)	35	203	0.513116 (10)	5	135		
229R1-66-71	1102.29	0.702566 (8)	200	180	0.513090 (30)	3	131	0.702744 (8)	40	200	0.513155 (10)	10	93		
242R2-35-39	1174.37	0.702488 (9)	200	240	0.513099 (44)	2	79	0.702941 (10)	50	333	0.513137 (12)	17	81		
249R1-54-56	1197.25	0.702564 (9)	200	200	0.513134 (30)	3	83	0.702719 (10)	60	200	0.513177 (16)	12	58		
250R1-83-87	1202.35				0.513019 (184)	1	40	0.702836 (9)	30	301	0.513157 (20)	7			
250R2-60-66	1203.59	0.702530 (9)	200	200	0.513236 (116)	3	84				0.513235 (22)	20	121		
251R1-60-65	1206.93	0.702569 (9)	150	181				0.703256 (60)	10	88	0.513172 (17)	4	136		
251R3-59-62	1209.77							0.704269 (18)	15	241	0.513179 (16)	5	136		
252R4-3-6a	1215.43	0.702612 (6)	170	340	0.513174 (33)	2	106	0.702920 (9)	30	208	0.513207^{+} (23)	5	84		
252R4-3-6b	1215.43	0.702633 (8)	200	192				0.703130 (16)	80	155	0.513230 (109)	16	45		
252R4-3-6c	1215.43							0.707908 (11)	49	134	0.512857 (18)	10	67		
253R1-40-41	1216.31													0.702618 (8)	0.513204 (9)
253R3-0-3	1218.63													0.702600 (10)	
253R3-45-78	1219.07							0.702927 (8)	15	222	0.513151 (15)	2	97		
257R1-95-100a	1236.08	0.702594 (9)	200	200	0.513048 (56)	3	64	0.702884 (9)	30	240	0.512800^{+} (15)	5	73		
257R1-95-100b	1236.08	0.702574 (15)	200	119	0.513088 (49)	6	75	0.707341 (11)	41	103	0.512927 (38)	11	68		
257R1-95-100c	1236.08							0.706109 (12)	82	193	0.513100 (16)	22	65		
257R1-95-100d	1236.08							0.703154 (50)	44	63	0.513192 (26)	12	55		

Table S1. *Continued*

Sample	depth	Plagioclase						Clinopyroxene						Whole rock	
	(mbsf)	$^{87}Sr/^{86}Sr$	Sr*	*n*	$^{143}Nd/^{144}Nd$	Nd*	*n*	$^{87}Sr/^{86}Sr$	Sr*	*n*	$^{143}Nd/^{144}Nd$	Nd*	*n*	$^{87}Sr/^{86}Sr$	$^{143}Nd/^{144}Nd$
260R1-14-16	1249.65													0.702664 (7)	0.513205 (7)
268R2-78-81	1290.03	0.702574 (8)	300	200				0.702865 (12)	35	227	0.513175 (17)	10	100		
268R3-6-12	1290.69				0.513301 (104)	2	73	0.702937 (9)	30	380	0.513194 (12)	10	108		
287R1-6-8	1377.67													0.702779 (8)	0.513191 (9)
292R1-75-77	1397.56				0.513169 (136)	1	80	0.703858 (14)	40	227	0.513168 (30)	9	39		
1310-A1-0-13	0.07													0.702576 (9)	0.513214 (11)
1310-A1-13-19	0.16													0.702567 (10)	0.513210 (11)
1310-B1R1-0-5	0.03													0.702572 (8)	0.513203 (10)
1310-B1R1-62-69	0.66													0.702560 (9)	0.513207 (16)
1310-B1R1-139-143	1.41													0.702572 (9)	0.513198 (9)
1311-AR1-0-9	0.05													0.702515 (10)	0.513220 (11)
1311-AR1-48-54	0.51													0.702528 (8)	0.513223 (9)
1311-AR1-99-104	1.02													0.702525 (9)	0.513225 (11)
1311-AR1-136-142	1.39													0.702499 (5)	0.513226 (9)

2 SE (in parentheses) are given in terms of least unit cited: e.g., 0.702643 (8) represent 0.70264 ± 0.000008.

n: number of cycles for each analyses

* Amount of Sr and Nd (in ng) analysed calculated from Sr and Nd concentration and estimated volume of milled mineral

+ $^{143}Nd/^{144}Nd$ ratios uncorrected for Sm: 0.512936±31 for 149R2-68-71a, 0.513169±19 for 252-R4-3-6a and 0.512783±15 for 257R1-95-100a.